Available online at www.sciencedirect.com
ScienceDirect
Applied Surface Science 254 (2008) 3767–3773
applied surface science
www.elsevier.com/locate/apsusc

High surface area thermally stabilized porous iron oxide/silica nanocomposites via a formamide modified sol–gel process

Kamal M.S. Khalil [a,*], Salah A. Makhlouf [b]

[a] Department of Chemistry, Faculty of Science, Sohag University, Sohag, P.O. Box 82524, Egypt
[b] Department of Physics, Faculty of Science, Assiut University, Assiut, P.O. Box 71516, Egypt

Received 2 October 2007; received in revised form 28 November 2007; accepted 28 November 2007
Available online 23 December 2007

Abstract

Iron oxide/silica (Fe:Si as 1:10 atomic ratio) composite materials have been prepared by calcination for 3 h at different temperatures (400–900 °C) of xerogel precursor obtained via a formamide modified sol–gel process. The process involved TEOS and iron(III) nitrate, nitric acid and formamide. Genesis of the composite materials from the xerogel precursor has been investigated by TGA, DSC, FTIR, XRD, SEM and EDX. Results indicated that all the calcined composites are mainly composed of amorphous iron oxide dispersed as finely divided particles in amorphous silica matrixes. Nitrogen adsorption/desorption isotherms revealed a reversible type I of isotherms indicative of microporosity. However, high S_{BET} surface area and microsporosity were observed for the calcined composite materials (e.g. $S_{BET} = 625\ m^2\ g^{-1}$, and $S_{\alpha s} = 556\ m^2\ g^{-1}$ for the composite calcined at 400 °C). Formation of the porous texture was discussed in terms of the action of formamide, which enhanced strengthening of the silica gel network during evaporation of the more volatile components within the composite body during the drying process.

Keywords: Fe_2O_3/SiO_2; Iron oxide/silica; Sol–gel; Nanocomposite; Formamide

1. Introduction

Oxide composites are very important as humidity sensing materials [1–3]. Iron oxide/silica, Fe_2O_3/SiO_2, nanocomposites have recently attracted increasing attention due to their interesting properties and applications in sensing, catalysis and magnetism [4–6]. Properties of Fe_2O_3/SiO_2 materials depend on the nature of the interaction between iron oxide and silica [7]. However, for most applications, effective composites must show porous texture of high surface area and thermal stability [8–10].

Sol–gel process has been known as a successful approach for synthesis of nanocomposites of the titled material, either by dispersing co-precipitated iron oxide particles in different sol–gel matrices or by homogenous precipitation of iron oxide nanoparticles during the matrix formation [5,11–13]. However, there are many parameters in the sol–gel process that need to be controlled in order to obtain the optimum particle and pore size distribution [11,14,15]. Several sol–gel preparations have utilized TEOS as a source for SiO_2, but different precursors for Fe_2O_3 phase were implemented. Thus, using $Fe(OC_2H_5)_3$ [16], or acetylacetonate [12,17] produces amorphous iron oxide upon calcinations at $\leq$700 °C, whereas calcinations at higher temperatures led to the formation of α-Fe_2O_3. Using iron(III) nitrate dissolved in ethylene glycol produces γ-Fe_2O_3 which is stable up to 650 °C [18]. Using TEOS and iron(III) nitrate in alcoholic acidic media under a long gelation condition [5] produced amorphous products for samples treated up to 600 °C, while at higher temperatures crystalline iron oxide phases were obtained.

For the preparation of porous composites exhibiting large surface areas and porosity, supercritical drying method has been implemented [12,19]. However, the use of drying control chemical additives (DCCA) can be considered as an alternative facile approach for the preparation of high surface area porous materials. Formamide, $HCONH_2$, is a common DCCA and its action on the sol–gel process of TEOS (or TMOS) has been extensively investigated [20–24]. Recently, a formamide modified sol–gel process has been employed to synthesize monolithic samples of γ-iron oxide nanoparticles within a

* Corresponding author. Fax: +20 93 4601 159.
E-mail address: kamal.khalil@sci.sohag.eud.eg (K.M.S. Khalil).

0169-4332/$ – see front matter © 2007 Elsevier B.V. All rights reserved.
doi:10.1016/j.apsusc.2007.11.066

transparent SiO_2 matrix [24]. The action of formamide as a DCCA may be considered to strengthen the gel by maximizing the extent of condensation, coarsening of microstructure and strengthening of the network via providing a medium through which the more volatile components (water and alcohol) can diffuse [25]. However, while modification with formamide has been frequently reported in the sol–gel literature, microstructure and surface texture studies for the materials obtained by calcination of the formamide-modified dried gels are rare.

The present article aims at preparation and characterization of Fe_2O_3/SiO_2 composite powder materials produced from a fomamide modified sol–gel precursors, which target application as humidity sensing materials. The merit of SiO_2 in this regard is its compatibility with current microelectronics industry [26]. The work aims at formation of porous composites, of high surface area and high thermal stability.

2. Experimental

2.1. Materials and preparations

Tetra-ethyl orthosilicate (TEOS), $Si(C_2H_5O)_4$; formamide, $HCONH_2$; ethanol, C_2H_5OH; nitric acid, HNO_3; and iron(III) nitrate, $Fe(NO_3)_3{\cdot}9H_2O$ were high purity reagents product of Aldrich Chem. Co. (USA). All chemicals were pursued and used as received.

Preparation of Fe_2O_3/SiO_2 composite containing as 1:10 Fe:Si atomic ratio (equivalent to Fe_2O_3/SiO_2 mass% = 13.3; $Fe_2O_3/(Fe_2O_3 + SiO_2)$ mass% = 11.7) was carried out from TEOS, formamide, ethanol, and 1.0N nitric acid aqueous solution. The mixing molar ratio of TEOS:$HCONH_2$:-C_2H_5OH:HNO_3 (1N aq) was 1:1:4:0.02. After mixing, iron(III) nitrate (s) was added to the above solution. The mixture was stirred for 2 h at 40 °C. The mixture was aged for three days, where a transparent reddish dense gel was formed. The formed gel was dried at 60 °C for 24 h period, then crunched and allowed for further drying, where the temperature was increased gradually to 120 °C and kept at this temperature for 24 h. The produced xerogel material is termed as the uncalcined composite. Portion of the later-dried material were calcined in a muffle furnace from room temperature to 400 °C at 1 °C min^{-1}, then the temperature was allowed to rise to the target temperature 600, 800, or 900 °C, at 10 °C min^{-1} (or just kept at 400 °C) and subjected to further calcinations for 3 h isothermally at the target temperature. The produced materials are termed as the calcined composites.

2.2. Techniques

2.2.1. Thermal analyses

A Thermal Analyst 2000 TA instrument (USA) controlling a 2050 thermogravimetric analyzer (TGA) and 2010 differential scanning calorimeter (DSC) was used. For TGA measurements, a ceramic sample boat was used with samples weighing 10.0 ± 0.1 mg. Data recorded upon heating up to 600 °C at 10 °C min^{-1} and in a stream (40 ml min^{-1}) of N_2 or O_2 gas atmosphere. For DSC measurements, a sample size of 5.0 ± 0.1 mg was heated up to 500 °C in a covered aluminum sample pan at 10 °C min^{-1} and a flow of 40 ml min^{-1} of N_2 gas.

2.2.2. Fourier transform infrared (FTIR)

FTIR spectroscopy for the test materials was carried out using KBr disc technique using a Fourier transform infrared spectrometer, model Shimadzu-FTIR800 (Japan), in the range 4000–400 cm^{-1}, with 40 scans and a resolution of 4 cm^{-1}.

2.2.3. X-ray diffraction (XRD)

XRD patterns were obtained using a Philips PW1700 diffractometer at room temperature. Diffraction patterns were obtained using Cu K_α radiation and graphite monochromator ($\lambda = 0.154$ nm) with automatic divergent slit. The resultant patterns were matched with standard data [27] for the purpose of phase identification.

2.2.4. Scanning electron microscopy (SEM) and energy dispersive X-ray analysis (EDX)

SEM micrographs were obtained using a Jeol microscope Model JSM-5600. EDX patterns were obtained via an Oxford EDX system for elemental analysis, the system was combined with the microscope. SEM samples were coated with gold before investigation.

2.2.5. Nitrogen adsorption/desorption isotherms

N_2 isotherms were measured at −196 °C according to the recommendations of the IUPAC [28] using a model ASAP 2010 instrument (Micromeritics Instrument Corporation, USA). Prior to measurement, all samples were outgassed for 2 h at 250 °C to 0.1 Pa. Specific surface area, S_{BET}, and c_{BET} constant were calculated by applying the BET equation [29]. The average pore width P_W was calculated from the ratio $4V_p/S_{BET}$, where V_p is the specific pore volume. Microporosity was assessed via α_s-method [30,31] using the standard data for nonporous silica [32]. Total pore volume, V_p was calculated at $P/P_0 = 0.95$.

3. Results and discussion

3.1. Thermal analyses

TGA and DTG curves for the uncalcined composite carried out in flow of N_2 atmosphere are shown in Fig. 1(a). Weight loss, WL, amount of 34.7%, was recorded upon heating over the range of room temperature (RT) to 600 °C. Most of the recorded WL (33.2%) occurred below 320 °C, whereas over the region of 320–600 °C a gradual WL amount of 1.5% was observed. DTG profile shows a strong peak through the region 90–320 °C, which maximize at 225 °C but shows an unresolved feature around 150 °C and a shoulder at 265 °C. Results obtained in flow of O_2 atmosphere for the uncalcined composite are shown in Fig. 1(b). WL amount of 42.7% was recorded upon heating over the range of RT–600 °C, in flow of O_2. DTG profile (obtained in flow of O_2) shows three peaks at 136, 172, 229 °C and a slim shoulder at 262 °C. Instead of the unresolved

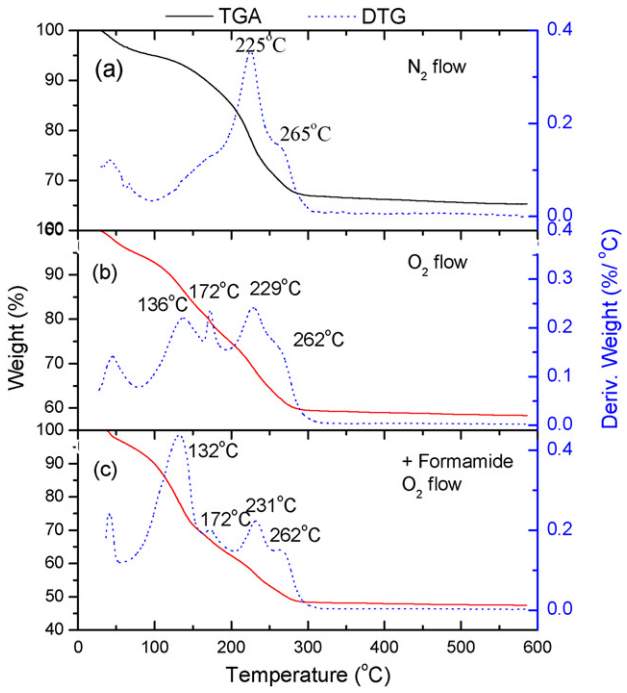

Fig. 1. TGA and DTG curves for the uncalcined Fe_2O_3/SiO_2 precursor (a) carried out in flow of N_2 atmosphere, (b) in flow of O_2 atmosphere and (c) mixed with formamide and carried out in flow of O_2 atmosphere as indicated in the text.

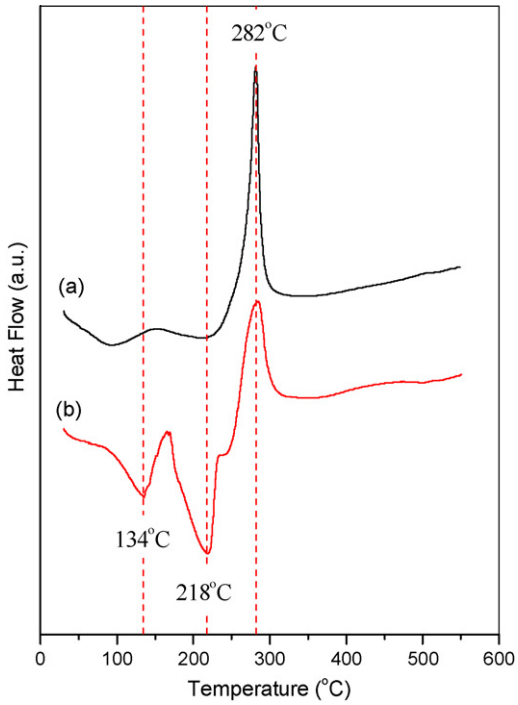

Fig. 2. DSC curves carried out in flow of N_2 atmosphere for samples of the uncalcined Fe_2O_3/SiO_2 precursor (a) pure, and mixed with formamide as indicated in the text (b).

feature, which was observed around 150 (in N_2 flow), two peaks at 136 and 172 °C were observed in flow of O_2, which suggests association of an oxidative decomposition process.

Fig. 1(c) shows the results obtained for the uncalcined composite physically mixed with formamide (formamide:uncalcined composite, respectively, as 3.2 mg:13.6 mg) in flow of O_2. WL amount of 52.6% was recorded over the range of RT–600 °C. Results indicated that all peaks remain at the same positions and only the relative intensity changes. Thus, indicating association of the observed peaks to the presence of formamide. Noting that none of above peaks were observed for the xerogel obtained by hydrolysis of TEOS in absence of formamide [33]. The WL observed for the present uncalcined composite 34.7% (in N_2), or 45.4% (in O_2), is larger than the WL value (<15%), which is normally observed for metal oxide/silica composite precursors hydrolyzed by ammonia solution in absence of modifiers [33,34].

It should be indicated that in the present method, the initial pH value for the reaction media was about 1 and the hydrolysis of formamide was preceded by the effect of H^+ and NO_3^- according to the following reaction [35]:

$$HCONH_2 + H_2O \xrightarrow{H^+,NO_3^-} HCOO^-NH_4^+ \leftrightarrow HCOOH + NH_3$$

However, since the total molar ratio of H^+ ions and other acidic species is much less than that of formamide, the final pH should remain close to that of formamide (about 5.0) [22]. Therefore, the increased WL percentage below 320 °C, for the present precursor material is mainly due to the contamination with the modifying species that are present in the processing media in addition to possible minor amounts of formamide hydrolysis products (such as NH_4^+ and HCOOH). Whereas, WL observed over the range of 320–600 °C (1.5%) may be attributed to further dehydroxylation and decarbonization during evolution of the composite material from its precursor.

DSC results for the uncalcined composite material in flow of N_2 atmosphere are shown in Fig. 2(curve a). The curve shows three peaks at 100 °C (endothermic), 218 °C (endothermic) and 282 °C (exothermic). The first endothermic peak is mainly assignable for desorption of water and low temperature volatile species (as shown by FTIR results below). DSC for a sample prepared by physical mixing of the precursor with formamide (precursor:formamide as 5.0 mg:2.5 mg) is shown in Fig. 2(curve b). Again, results indicated that all peaks remain at the same positions and only the relative intensity changes.

The above DSC data help explaining of the TGA results, thus, the 136 and 172 °C DTG peaks appear in flow of O_2, which was not resolved in flow of N_2 (TGA and DSC), can be assigned respectively to dehydration process and combustion of free formamide (which, characterized by a close flash point at 150 °C in closed cup). On the other hand, the DSC (N_2) peak at 218 °C is related to the DTG peak shown at ~225 °C either in N_2 or O_2 atmosphere and may be assigned to desorption of formamide, which characterized by a boiling point at 212 °C. Similar thermal events were recently observed, through evolution of SiO_2–P_2O_5 from a formamide containing gel [36]. Finally, the DSC exothermic peak at 282 °C, which could be related to the small DTG shoulder at 265 °C, may be due to decomposition of adsorbed nitrates and/or organic species. Recently, however, it has been reported that DSC profile of pure

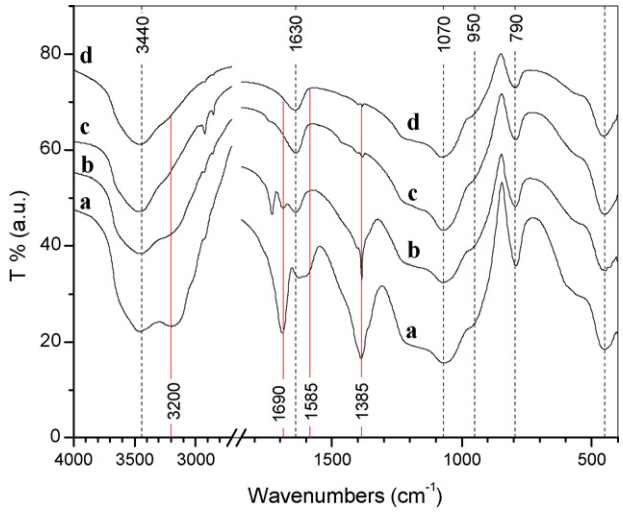

Fig. 3. FTIR spectra for the uncalcined Fe_2O_3/SiO_2 precursor (a) dried at 120 for 24 h, (b) dried at 150 for 24 h, along with samples heated at 250 °C (c) and 600 °C (d).

Fe_2O_3 [4] showed a similar peaks at ~280 °C in the flow of N_2 atmosphere (absence of O_2), which was ascribed to the transformation of Fe_2O_3 from amorphous into γ-Fe_2O_3.

3.2. FTIR spectroscopy

Fig. 3 shows FTIR spectra for the uncalcined composite (dried at 120 °C for 24 h), spectra a. Three other spectra for the samples obtained by gradual heating of the uncalcined composite at 10 °C min^{-1}, up to 150 °C (spectra b), up to 250 °C (spectra c), or up to 600 °C (spectra d). The samples were kept at the target temperatures for 10 min, except the first one, which was left for 24 at 150 °C, before quenching to RT.

FTIR spectrum for the uncalcined composite, Fig. 3, spectrum (a), principally shows a typical group of bands, which are persistent for the samples heated at 150, 250, and 600 °C as shown by the dashed lines on Fig. 3. This group of bands has characteristics for silica gel and similar to those formed in the case of hydrolysis of TEOS by ammonia solution in alcoholic medium [33,34]. Accordingly, the bands at 3440 and 1630 cm^{-1} are assignable to the ν(O–H) mode of (H-bonded), and δ(O–H) mode of water molecules, respectively. The bands at 1070 and 790 cm^{-1} are assignable to ν_{as}(Si–O–Si) and ν_s(Si–O–Si) modes, respectively. The small shoulder band at 950 cm^{-1} is assignable to ν(Si–OH). Note that, the latter band normally appears as a sharp one in absence of formamide. This may indicate that presence of formamide affect the behaviour of surface (Si–OH) groups. Finally, the band observed at 450 cm^{-1} is assignable to the δ(Si–O–Si) mode. In addition to the above group of bands characteristic for silica gel, some other bands can be recognized for the uncalcined composite, Fig. 3 spectrum (a). These bands may be related to the modifiers and/or their reaction products and are assignable as follows [37]. The strong band at 1385 cm^{-1} is assignable for NO_3^- group. The ~3200 cm^{-1} band is assigned to ν(N–H) of free and/or H-bonded formamide; and the 1690 cm^{-1} (sharp) band is assigned to ν(C=O) of free formamide.

Upon increasing the drying temperature up to 150 °C, spectrum (b) of Fig. 3, bands related to free formamide (~3200 and 1690 cm^{-1}) were removed, and a small sharp band at 1730 cm^{-1} related to H–bonded ν(C=O) of free formamide is evident (this band was not clear for the case 120 °C dried material (spectrum a), probably due to shielding by the strong 1690 cm^{-1} band). However, the 1385 cm^{-1} band related to NO_3^- still present as shown from the spectrum. For the sample heated up to 250 °C, spectrum (c), the 1385 and 1735 cm^{-1} bands disappeared indicating the removal of bonded formamide and nitrate species. For the sample heated at 600 °C, spectrum (d), there is no change except for the removal of C–H moieties, thus, a spectrum typical for fully hydrolyzed silica gel was obtained.

In this discussion it is important to indicate the noticeable absence of any characteristic bands for the Si–O–Fe bond, which normally manifest itself at 857 cm^{-1} [11]. However, possible formation of iron formate cannot be ruled out. Even though, if any iron(III) formate, $[Fe_3O(HCOO)_6]^+HCOO^-$, was formed, it would decompose completely before 330 °C [38].

3.3. XRD diffraction

XRD patterns for the uncalcined composite, along with the composites calcined at 600 °C/3 h and at 900 °C/3 h are shown in Fig. 4. The composite patterns, generally show amorphous nature and show halo patterns, near $2\theta = 25°$, characteristic for amorphous silica. The patterns dictation by the amorphous silica nature was probably due to the small percentage of iron oxide in the composite materials. No clear peaks were detected for the iron oxide phase at the different calcination temperatures of the composite. Nevertheless, the standard lines for the expected phases (maghemite, γ-Fe_2O_3 and hematite, α-Fe_2O_3) [27] were tested as shown by the inserted symbols and lines in Fig. 4. Accordingly, there is no evident peak

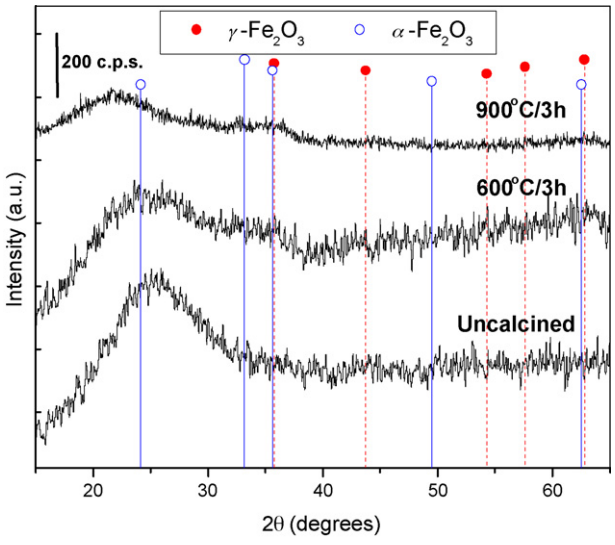

Fig. 4. XRD patterns for the uncalcined Fe_2O_3/SiO_2 precursor, along with the Fe_2O_3/SiO_2 composite calcined for 3 h at 600 °C and 900 °C, as indicated. Standard diffraction data for γ-Fe_2O_3 and α-Fe_2O_3 are inserted. Where, symbols and dropped lines were used to indicate position and relative heights for the standard diffraction data in each case.

Table 1
Texture characteristics for the calcined Fe_2O_3/SiO_2 composite materials

Calcination	S_{BET} ($m^2\ g^{-1}$)	c_{BET}	$S_{(s}$(mic) ($m^2\ g^{-1}$)	$S_{(s}$(ext) ($m^2\ g^{-1}$)	V_p ($cm^3\ g^{-1}$)	P_w[a] (nm)	Silica particles diameter[b] (nm)
400 °C/3 h	625	206	556	5	0.330	2.1	3.9
600 °C/3 h	557	156	533	3	0.287	2.1	4.4
800 °C/3 h	352	96	379	4	0.191	2.2	6.9
900 °C/3 h	111	70	130	2	0.067	2.4	21.7

[a] Calculated as $4V_p/S_{BET}$.
[b] Calculated assuming the theoretical bulk densities of the composite constituents.

matching and/or broadening at the tested positions. This suggests that iron oxide particles are amorphous and/or smaller than the detection limits of the XRD method (5 nm) [4]. In a similar investigation that utilized TEOS and iron(III) nitrate precursors without any modifiers, completely amorphous Fe_2O_3 was obtained after calcinations at 600 °C, but crystallizes if calcined at higher temperatures [5]. The absence of crystalline hematite at 900 °C in the present study could be explained in terms of the low content of iron oxide, which prevents formation of larger nanoparticles that easily convert into α-Fe_2O_3 [39]. The above discussion suggests that the composite materials are composed of amorphous-iron oxide/silica, i.e. finely divided amorphous iron oxide particles are formed and stabilized by the porous texture of the formed silica gel (as shown below), which hinders movement and coalescence of nano Fe_2O_3 particles.

3.4. Nitrogen adsorption

Nitrogen adsorption/desorption isotherms on the different calcined materials are shown in Fig. 5. The isotherms are classified according to the IUPAC [28] as reversible type I type of isotherm, characteristic for microporous materials, and show no appeasable hysteresis loops. However, according to the extended classification of adsorption isotherms [40], the isotherms are designated as type 1b, the gradual approach to the plateau at $P/P_0 \sim 0.4$ is an indication of a wide distribution of micropores. S_{BET} surface area values amount to 625, 557, 352 and 111 $m^2\ g^{-1}$ were obtained for the materials calcined at 400, 600, 800 and 900 °C, respectively, as shown in Table 1. Alpha-s, α_s, analysis of the adsorption branches of the isotherms are shown in Fig. 6. Values of micropore surface area, α_s(mic) and external surface area α_s(ext) obtained from the slopes of the α_s-plots at the lower and the higher range, respectively, were estimated. Thus, α_s(mic) values amounting to 556, 533, 379 and 130 were obtained for the composites calcined at 400, 600, 800 and 900 °C, respectively, as shown in Table 1. However, smaller α_s(ext) values, $\leq 5\ m^2\ g^{-1}$, were obtained for all of the test materials. This result confirms the predominant microporous nature of the test materials. Values of total pore volume, V_p, was found to decrease with the increase

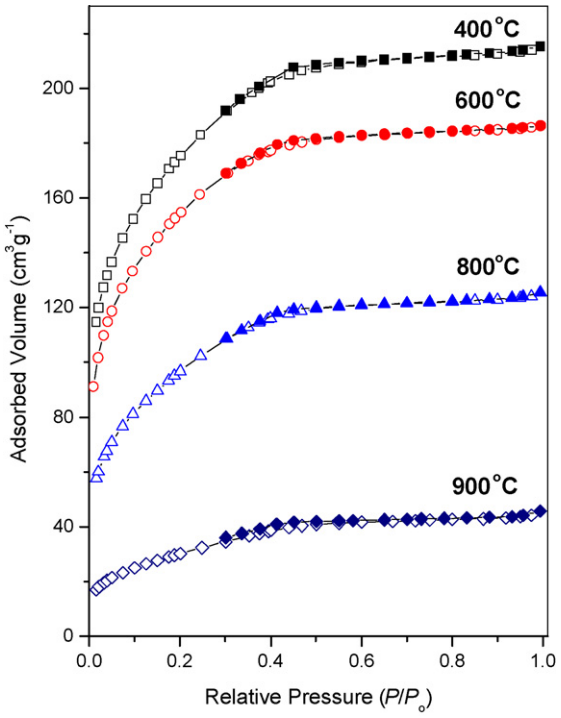

Fig. 5. Nitrogen adsorption/desorption isotherms for the Fe_2O_3/SiO_2 composite materials calcined for 3 h at 400, 600, 800 and 900 °C, as indicated. Open symbols denote adsorption and closed symbols denote desorption.

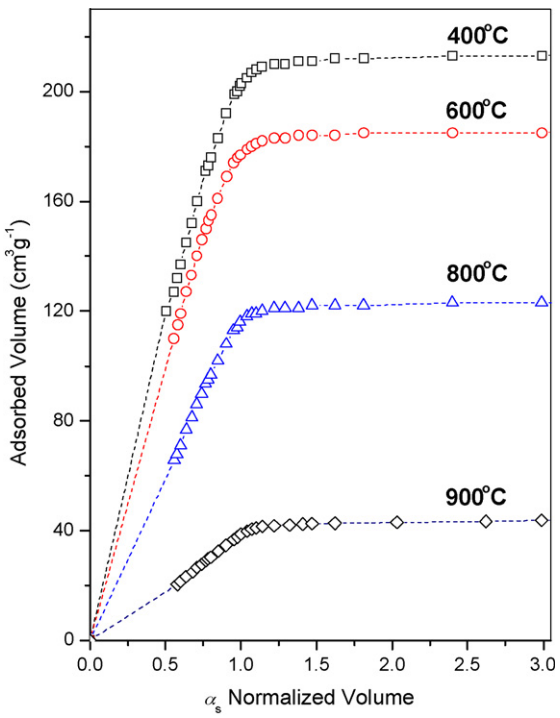

Fig. 6. Plots of Alpha-*s* test method obtained with the adsorption isotherms of the Fe_2O_3/SiO_2 composite materials calcined for 3 h at 400, 600, 800 and 900 °C.

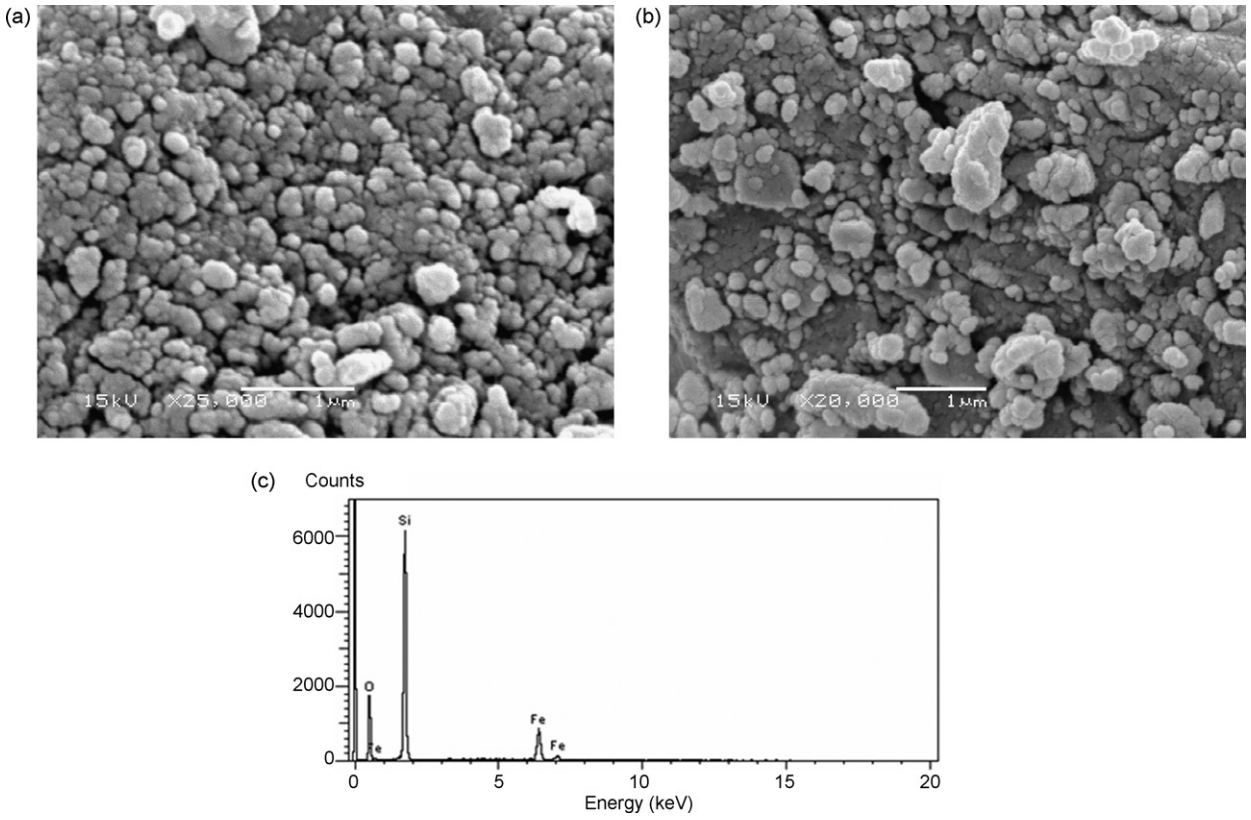

Fig. 7. SEM micrographs for (a) the uncalcined Fe_2O_3/SiO_2 precursor and for (b) the Fe_2O_3/SiO_2 composite calcined for 3 h at 600 °C as well as (c) EDX analysis obtained with the calcined composite shown in image (b).

in the calcination temperature as shown in Table 1. Average pore width, P_w, was estimated from the relation ($4V_p/S_{BET}$), since the BJH method is not applicable due to the microporous nature of the materials. Thus, P_w values above 2.0 nm were obtained for all the calcined composites. Furthermore, based on the S_{BET} values and assuming the theoretical bulk densities of the composite constituents, the equivalent spherical particle diameter of the composite primary particles were theoretically estimated as shown in Table 1. Particle diameter was found to be around 4 nm for the samples calcined at 400 °C and 600 °C, approaching ~7 nm for the material calcined at 800 °C and jump to >20 nm for the material calcined at 900 °C. The estimated values for particle diameter represent size for silica rather than iron oxide particles, since the former is the major phase, which can grow in size by coalescence. This result is a typical for silica gel structure, which composed of aggregates of very small nanosized silica primary particles.

3.5. Electron microscopy

SEM micrographs for the uncalcined and the calcined (at 600 °C for 3 h) composites are shown in Fig. 7(a) and (b), respectively. The general morphology of the uncalcined composite showed a case of spherical-like aggregates (secondary particles) of variable size ≤0.1 μm in diameter, which is of course composed of nanosized aggregates of primary particles. As shown on Fig. 7(a), some of the spherical-like secondary particles, themselves, are consolidate in larger agglomerates of different shapes and variable size (≤0.4 μm). SEM micrograph for the calcined composite, Fig. 7(b), shows a similar morphology to that shown above, nevertheless more clear grain boundaries and relatively more aggregation of the spherical-like secondary particles can be observed. EDX analysis obtained with the calcined composite is shown in Fig. 7(c), which indicates the inclusion of iron species in silica matrix, with a ratio very close to the nominated 1:10 Fe:Si atomic ratio. This confirms that iron oxide particles are present as finely divided nanosized particles (below the detection limits of the employed microscope) dispersed within the primary nanosized silica particles.

Therefore, formamide effectively affected microstrcure and surface texture of the produced calcined composites. This can be explained in terms of DCCA action of formamide, which under neutral conditions involve increasing hydrogen bonding and solvent viscosity [20]. Whereas, under acid catalyzed conditions formamide actions are controlled by its hydrolysis and the progressive increase of the solution pH with time [21]. This leads to effective hydrolysis in the initial reaction stages (at low pH) followed by efficient condensation in the final reaction stages (at high pH). This leads to the formation of strengthen gel that upon drying and calcinations at high temperatures produce thermally stabilized microporous texture.

4. Conclusions

Microporous Fe_2O_3/SiO_2 nanocomposite materials were obtained by calcination of the xerogel obtained via a formamide modified sol–gel process. The observed porosity was related to the modification process, which takes the advantages of formamide as a pH controller and DCCA. Formamide, which bonds itself to the silica gel surface modified the gelation and drying processes, led to strengthening of the silica gel network during evaporation of the more volatile components without reorganization into a particular structure. Thus, formamide led to creation of microporosity and thermal stability upon calcination. Therefore, the nano sized amorphous iron oxide particles are stabilized within the porous texture, which prevented them from coalescence and growth upon calcinations at higher temperatures. The present powder composites showed higher surface area and amorphous phase stability higher than similar composites prepared by formamide-free so–gel processes.

References

[1] S.A. Makhlouf, K.M.S. Khalil, Solid State Ionics 164 (2003) 97.
[2] M.M. Ahmad, S.A. Makhlouf, K.M.S. Khalil, J. Appl. Phys. 100 (2006) 094323.
[3] R. Sundaram, K.S. Nagaraja, Mater. Res. Bull. 39 (2004) 581.
[4] L. Machala, R. Zboril, A. Gedank, J. Phys. Chem. B 111 (2007) 4003.
[5] G. Ennas, A. Musinu, G. Piccaluga, D. Zedda, D. Gatteschi, C. Sangregorio, J.L. Stanger, G. Concas, G. Spano, Chem. Mater. 10 (1998) 495.
[6] T. Nakamura, Y. Yamada, K. Yano, J. Mater. Chem. 16 (2006) 2417.
[7] S.G. Marchetti, M.V. Cagnoli, A.M. Alvarez, N.G. Gallegos, J.F. Bengoa, A.A. Yeramian, R.C. Mercader, J. Phys. Chem. Solids 58 (1997) 2119.
[8] D.K. Yi, S.S. Lee, J.Y. Ying, Chem. Mater. 18 (2006) 2459.
[9] H. Yang, Q. Lu, F. Gao, Q. Shi, Y. Yan, F. Zhang, S. Xie, B. Tu, D. Zhao, Adv. Funct. Mater. 15 (2005) 1377.
[10] S. Sato, R. Takahashi, T. Sodesawa, R. Tanaka, Bull. Chem. Soc. Jpn. 76 (2003) 217.
[11] E.M. Moreno, M. Zayat, M.P. Morales, C.J. Serna, A. Roig, D. Levy, Langmuir 18 (2002) 4972.
[12] C.-T. Wang, S.-H. Ro, Appl. Catal. A: Gen 285 (2005) 196.
[13] C. Cannas, D. Gatteshi, A. Musinu, G. Piccaluga, C. Sangregorio, J. Phys. Chem. B 102 (1998) 7721.
[14] S. Solinas, G. Piccaluga, M.P. Morales, C.J. Serna, Acta Mater. 49 (2001) 2805.
[15] D. Niznansky, N. Viart, J.L. Rehspringer, J. Sol–Gel Sci. Technol. 8 (1997) 615.
[16] M. Guglielmi, G. Principi, J. Non-Cryst. Solids 48 (1982) 161.
[17] K. Tanaka, K. Kamiya, M. Matsuoka, T. Yoko, J. Non-Cryst. Solids 94 (1987) 356.
[18] T. Ida, H. Tsuiki, A. Ueno, K. Tohji, Y. Udagawa, K. Iwai, H. Sano, J. Catal. 106 (1987) 428.
[19] M. Popovici, M. Gich, A. Roig, L. Casas, E. Molins, C. Savii, D. Becherescu, J. Sort, S. Surinach, J.S. Munoz, M.D. Baro, J. Nogues, Langmuir 20 (2004) 1425.
[20] G. Orcel, L.L. Hench, J. Non-Cryst. Solids 79 (1986) 177.
[21] H. Rosenberger, H. Burger, H. Schutz, G. Scheler, G. Maenz, Z. Phys. Chem. Neue Folge 153 (1987) 27.
[22] N. Viart, J.L. Rehspringer, J. Non-Cryst. Solids 195 (1996) 223.
[23] Y.T. Lee, H.H. Jen, J. Non-Cryst. Solids 342 (2004) 39.
[24] D. Ortega, J.S. Garitaonandia, C. Barrera-Solano, M. Domínguez, Sens. Lett. 5 (2007) 69.
[25] C.J. Brinker, G.W. Scherrer, In Sol–Gel Science: The Physics and Chemistry of Sol–Gel Processing, Academic Press, San Diego, 1990, pp. 500.
[26] Z. Chen, C. Lu, Sens. Lett. 3 (2005) 274.
[27] JCPDS, International Centre for Diffraction Data, PCPDFWIN, JCPDS-ICDD, 1995.
[28] K.S.W. Sing, D.H. Everett, R.A.W. Haul, L. Moscou, R.A. Pierotti, J. Rouquerol, T. Siemieniewska, International Union of Pure and Applied Chemistry, IUPAC, Pure Appl. Chem. 57 (1985) 603.
[29] B. Brunauer, P.H. Emmett, P.H.E. Teller, J. Am. Chem. Soc. 60 (1938) 309.
[30] K.S.W. Sing, Chem. Ind. (1968) 829.
[31] F. Rouquerol, J. Rouquerol, K. Sing, Adsorption by Powders and Porous Solids, Academic Press, London, 1999, p. 176.
[32] S.J. Gregg, K.S.W. Sing, Adsorption, Surface Area and Porosity, Academic Press Inc., London, 1982, p. 93.
[33] K.M.S. Khalil, A.A. Elsamahy, M.S. Elanany, J. Colloid Interf. Sci. 249 (2002) 359.
[34] K.M.S. Khalil, L.A. Elkabee, B. Murphy, J. Colloid Interf. Sci. 287 (2005) 534.
[35] C.J. Brinker, G.W. Scherrer, In Sol–Gel Science: The Physics and Chemistry of Sol–Gel Processing, Academic Press, San Diego, 1990, p. 197.
[36] S.-P. Tung, B.-J. Hwang, J. Membr. Sci. 241 (2004) 315.
[37] I.A. Degen, Tables of Characteristic Group Frequencies for the Interpretation of Infrared and Raman Spectra, Acolyte Publ., Harrow, UK, 1997.
[38] F. Kenfack, H. Langbein, Thermochim. Acta 426 (2005) 61.
[39] I.K. Battisha, H.H. Afify, I.M. Hamada, J. Magn. Magn. Mater. 292 (2005) 4404.
[40] F. Rouquerol, J. Rouquerol, K. Sing, Adsorption by Powders and Porous Solids, Academic Press, London, 1999, pp. 339–342.